# Steady-state dissolution kinetics of goethite in the presence of desferrioxamine B and oxalate ligands: implications for the microbial acquisition of iron

Sing-Foong Cheah[a], Stephan M. Kraemer[b], Javiera Cervini-Silva[a], Garrison Sposito[a,*]

[a] *Division of Ecosystem Sciences, University of California, Berkeley, CA 94720-3110, USA*
[b] *Institute of Terrestrial Ecology, ETH-Zürich, CH-8952, Schlieren, Switzerland*

## Abstract

This paper reports an investigation of the effects of a trihydroxamate siderophore, desferrioxamine B (DFO-B), and a common biological ligand, oxalate, on the steady-state dissolution of goethite at pH 5 and 25 °C. The main goal of our study was to quantify the adsorption of the ligands and the dissolution of goethite they promote in a two-ligand system. In systems with one ligand only, the adsorption of oxalate and DFO-B each followed an L-type isotherm. The surface excess of oxalate was approximately 40 mmol kg$^{-1}$ at solution concentrations above 80 μM, whereas the surface excess of DFO-B was only 1.2 mmol kg$^{-1}$ at 80 μM solution concentration. In the two-ligand systems, oxalate decreased DFO-B adsorption quite significantly, but not vice versa. For example, in solutions containing 40 μM DFO-B and 40 μM oxalate, 30% of the DFO-B adsorbed in the absence of oxalate was displaced. The mass-normalized dissolution rate of goethite in the presence of DFO-B alone increased as the surface excess of the ligand increased, suggesting a ligand-promoted dissolution mechanism. In systems containing oxalate only, mass-normalized goethite dissolution rates were very low at concentrations below 200 μM, despite maximal adsorption of the ligand. At higher oxalate concentrations (up to 8 mM), the steady-state dissolution rate continued to increase, even though the surface excess of adsorbed ligand was essentially constant. Chemical affinity calculations and dissolution experiments with variation of the reactor flow rate showed that far-from-equilibrium conditions did not obtain in systems containing oxalate at concentrations below 5 mM. The dissolution rate in the presence of DFO-B at solution concentrations between 1 and 80 μM was approximately doubled when oxalate was also present at 40 μM solution concentration. The dissolution rate in the presence of oxalate at solution concentrations between 0 and 200 μM was increased by more than an order of magnitude when DFO-B was also present at 40 μM solution concentration. Chemical affinity calculations showed that, in systems containing DFO-B, goethite dissolution was always under far-from-equilibrium conditions, irrespective of the presence of oxalate. These results were described quantitatively by a model rate law containing a term proportional to the surface excess of DFO-B and a term proportional to that of oxalate, with both surface excesses being determined in the two-ligand system. The pseudo first-order rate coefficient in the DFO-B term has the same value as measured for goethite dissolution in the presence of DFO-B only, while the rate coefficient in the oxalate term must be measured in the two-ligand system, since it is only in this system that far-from-equilibrium conditions obtain. These latter conditions do not exist in the system containing oxalate only, but they do exist in the DFO-B/oxalate system because the siderophore is able to remove Fe(III) from all Fe–oxalate complexes rapidly, leaving the uncomplexed oxalate ligand in solution free to react again with the goethite

* Corresponding author.
*E-mail address:* gsposito@nature.berkeley.edu (G. Sposito).

surface. This synergy observed in the two-ligand system implies that the production of modest quantities of siderophore in the presence of very low concentrations of oxalate would be an extremely effective mechanism for the microbially induced release of Fe from goethite.

## 1. Introduction

The role of siderophores [σίδηρος(iron)+φέρω (carry)] in the acquisition of iron by fungi and bacteria has long been appreciated (Neilands, 1974; Cornell and Schwertmann, 1996; Albrecht-Gary and Crumbliss, 1998), but little quantitative understanding of the biogeochemistry of these microbial compounds is available. Kalinowski et al. (2000) have reviewed the few extant studies of siderophore-promoted mineral dissolution, noting particularly the unexpectedly modest enhancement of dissolution rates that siderophores produce and the existence of a "saturation effect" (plateau in the dissolution rate as a function of ligand concentration) for dissolution promoted by trihydroxamate siderophores. They concluded with a call for "careful, controlled experiments in chemical reactors" to improve understanding of siderophore biogeochemistry.

In a pioneering experiment with goethite ($\alpha$-FeOOH), Watteau and Berthelin (1994) observed the release of twice as much Fe in the presence of 126 $\mu$M desferrioxamine B (DFO-B), a common trihydroxamate siderophore (Crumbliss, 1991), as in the presence of HCl at pH 3 over a 28-day reaction. A 3 mM mixture of oxalic, malic, and citric acid at pH 3 released almost three times as much Fe as did HCl during the same period. However, on a per-mole basis, the siderophore was nearly 20 times more effective than were the aliphatic acids at releasing Fe from goethite. Similar data were obtained with other Fe-bearing minerals (Watteau and Berthelin, 1994).

Kraemer et al. (1999) also observed enhanced Fe release from goethite in the presence of 240 $\mu$M DFO-B at pH 6.5, concluding, in agreement with Holmén and Casey (1996, 1998) and Kalinowski et al. (2000), that coordination of the siderophore to an Fe(III) center at the mineral surface is a precursor to the dissolution process. Cocozza et al. (2001) compared the temperature dependence of goethite dissolution at pH 6.5 in the presence of 240 $\mu$M DFO-B with that of $Fe^{3+}$ complexation by the siderophore in aqueous solution, concluding that DFO-B coordinates with only a single hydroxamate group when binding to an Fe(III) center on the goethite surface, a possibility previously suggested previously by Holmén and Casey (1996, 1998).

Watteau and Berthelin (1994) noted that aliphatic acids at submillimolar concentrations typical for soils usually promoted greater Fe release from minerals than did DFO-B at typical micromolar concentrations. They speculated that the presence of both types of organic ligand could result in selective strategies for mobilizing Fe from minerals under a variety of soil conditions. In this paper, we take up the issue of combined ligand effects in presenting the results of adsorption and steady-state dissolution experiments involving goethite in the presence of DFO-B and the ubiquitous biological ligand, oxalate (Gadd, 2000). Our objective was to quantify the dissolution kinetics of goethite at varying concentrations of DFO-B, oxalate, and the two ligands in combination, so as to gain insight into their possible combined role in the microbial acquisition of Fe.

## 2. Materials and methods

### 2.1. Materials

The sample of desferrioxamine B used was the mesylate salt [$C_{25}H_{46}N_5O_8NH_3^+(CH_3SO_3^-)$], obtained initially from Sigma, but primarily from a sample produced by Ciba-Geigy (Desferal®) that was received as a gift from the Salutar Corporation. The unlabeled sample of oxalic acid ($C_2H_4O_2$) used was obtained from Aldrich (Cat. No. 24, 117-2; 99+%), whereas $^{14}C$-labeled oxalic acid was obtained from Sigma Radiochemicals [[(Cat. No. 31, 391-2, Lot No.

18H9466; specific activity 7.1 mCi mmol$^{-1}$ (Ci = curie)].

Solutions containing desferrioxamine B mesylate, oxalic acid, $^{14}$C-labeled oxalic acid, sodium perchlorate (GFS, ACS grade), MOPS buffer (3-[*N*-Morpholino]propanesulfonic acid; Sigma), MES buffer (2-[*N*-Morpholino]ethanesulfonic acid; Sigma), sodium hydroxide (Baker Analyzed Reagent Grade), perchloric acid (Fisher, Optima grade), Fe(III) perchlorate hexahydrate (GFS, ACS grade), or Fe ICP standard solution (Ultra Scientific) were prepared with high-purity 18 MΩ cm$^{-1}$ water (Milli-Q Plus, Millipore). The scintillation cocktail used for $^{14}$C analysis (Scintiverse) was obtained from Fisher.

Goethite (α-FeOOH) was synthesized using a method described by Schwertmann and Cornell (1991). Briefly, 180 ml of 5 M KOH solution were added rapidly with stirring to 100 ml of 1 M Fe(NO$_3$)$_3$ solution in a 2 l polyethylene flask. The resulting suspension was then brought to 2 l total volume with high-purity 18 MΩ cm$^{-1}$ water and heated at 70 °C for 60 h. The precipitated product was stored in suspension for a few months, centrifuged, washed with high-purity water, then freeze-dried. Powder X-ray diffraction and transmission electron microscopy confirmed that the synthesized solid was goethite. Its specific surface area (static BET method) was 35 ± 3 m$^2$ g$^{-1}$. Prior to the adsorption and dissolution experiments, a goethite stock suspension was prepared by sonicating a mixture of the freeze-dried precipitate with the background electrolyte solution for 1 min.

## 2.2. Dissolution experiments

Continuous-flow stirred tank reactors (Nagy et al., 1991; Kraemer and Hering, 1997) were used in the goethite dissolution experiments. The reactors were obtained from Cole-Parmer (Cat. No. E-02910-41), the cap and bottom being made with Delrin®, while the main reactor body was machined in Berkeley with Plexiglass®. The volume of the reactors was determined by carefully filling them with water (with a 0.025 μm filter in place) and measuring the additional mass. The median volume of the four reactors was 69.4 ± 0.3 ml.

The reactors were immersed in a constant-temperature water bath at 25 °C, with the entire apparatus wrapped in Al foil to exclude light during the experiments. A 0.025 μm mixed cellulose–acetate filter (Millipore) was placed at the outflow of each reactor to contain the goethite sample within it. The goethite concentration in the reactor was 10.0 g l$^{-1}$. The goethite slurry was mixed by a suspended magnetic stirrer (i.e., one that does not contact the bottom of the reactor). The stirring speed, monitored using a stroboscope, was maintained at 500 rpm. The flow rate in the reactors was controlled using a variable-speed peristaltic pump (Masterfex®) and was determined daily by collecting effluent over a fixed period of time and then dividing the volume of the effluent by the collection time. Pump tubing was replaced every 2–3 weeks, with no data collected for 2 days after replacement. Care was taken to ensure that there were no air bubbles trapped in the pump tubing or in the tubing connecting bottles containing the influent solutions to the reactors.

The composition of the influent solutions was 10 mM NaClO$_4$ at pH 5 mixed with oxalate (0–8000 μM) and/or DFO-B (0–80 μM). All experiments were conducted with MOPS buffer, except for those involving oxalate alone at concentrations between 200 and 8000 μM, which were conducted with MES buffer. Kraemer et al. (1999) have shown that the use of MOPS buffer has no significant effect on the dissolution rate of goethite. Yu et al. (1997) and Soares et al. (1999) also have found that MOPS and MES buffers are non-complexing ligands with trace metal ions. Effluent samples were collected daily, with one portion used for pH measurements. A second portion was stored in a refrigerator to be used weekly for measurement of total dissolved Fe concentration by inductively coupled plasma-atomic emission spectrometry (ICP-AES).

The mass-normalized steady-state dissolution rate of goethite was calculated as:

$$R = [\text{Fe}]_{\text{eff}} \frac{q}{m} \qquad (1)$$

where $[\text{Fe}]_{\text{eff}}$ is the total dissolved Fe concentration in the effluent (μM) under steady-state conditions, $q$ is the effluent flow rate (ml h$^{-1}$), and $m$ is the mass of goethite in the reactor (g). The resulting units of $R$ are then μmol kg$^{-1}$ h$^{-1}$. The standard deviation of $R$ values ($\Delta R$) was estimated as:

$$\Delta R = R \left[ \left( \frac{\Delta[\text{Fe}]_{\text{eff}}}{[\text{Fe}]_{\text{eff}}} \right)^2 + \left( \frac{\Delta q}{q} \right)^2 + \left( \frac{\Delta m}{m} \right)^2 \right]^{1/2} \qquad (2)$$

where $\Delta[Fe]_{eff}$ is the standard deviation of $[Fe]_{eff}$, etc. The minimum detectable $[Fe]_{eff}$ was 0.04 μM and the smallest dissolution rate measurable in our experiments was about 0.1 μmol kg$^{-1}$ h$^{-1}$.

### 2.3. Adsorption experiments

Adsorption of the organic ligands on goethite was investigated in batch mode in 10 mM NaClO$_4$ and 5 mM MOPS buffer, with samples open to the atmosphere at ambient temperature. A stock suspension containing 30.0 g l$^{-1}$ goethite was prepared and, for each adsorption experiment, 5 ml of the suspension and predetermined volumes of electrolyte and acid/base were placed in 30 ml amber HDPE bottles. Aliquots of stock solutions containing DFO-B (2 mM), oxalic acid (4 mM) and/or $^{14}$C labeled oxalic acid (1 μCi/ml; 133 μM) were then added to achieve the desired solution composition. The labeled oxalic acid aliquot was always added immediately after the nonlabeled oxalic acid. The order in which DFO-B and nonlabeled oxalate were added was randomized from sample to sample. The total volume of each sample was 15 ml, yielding solids concentration of 10.0 g l$^{-1}$. The samples were placed on a rotator for 1 h to equilibrate them before being filtered. The filtration process required about 20 min, so the actual equilibration time of a sample was nearly 100 min. This reaction time was optimized so that dissolved Fe would not be a substantial part of the equilibrated solution composition ($<10$ μM). Solution pH was measured immediately after all components were added (pH of the slurry) and after filtration (pH of the filtrate). There was no significant change of pH in all cases, the average sample pH being $5.06 \pm 0.07$.

The equilibrated samples were filtered with either a 0.05 μm (Millipore) mixed cellulose ester membrane filter or a 0.2 μm Nalgene® surfactant-free cellulose–acetate disposable syringe-filter, the latter being found to be just as effective as the 0.05 μm filter for our sample of goethite. Experiments with (goethite-free) blank solutions were conducted to check for loss of DFO-B or oxalic acid to container walls or to the filter. Because of the filter loss, which was typically on the order of a few percent of the ligand concentration in the filtrate, it was found prudent to pre-saturate the filter with the sample solution, then discard the first few milliliters of filtrate. For samples

filtered with a 0.05 μm mixed cellulose ester membrane filter, the first 2 ml of filtrate was discarded; for samples filtered with a 0.2 μm Nalgene brand surfactant-free cellulose–acetate disposable syringe-filter, the first 6 ml of filtrate was discarded. Experiments following this protocol showed negligible loss of DFO-B and oxalic acid in blank solutions.

The surface excess of the analyte (DFO-B or oxalic acid) was calculated by dividing the concentration loss (initial concentration minus the total ligand concentration in the filtrate) by the solids concentration. Errors in adsorbed concentration were estimated based on equating the sample coefficient of variation to the square root of the sum of squares of the coefficients of variation of constituent quantities in the definition of the surface excess, similarly to Eq. (2).

### 2.4. Analytical methods

The concentration of DFO-B in the filtrate from an adsorption experiment was analyzed with a Shimadzu UV-160 spectrophotometer at 439 nm as the Fe–DFO-B complex in the presence of excess Fe (Solinas, 1994; Cocozza et al., 2001). All spectrophotometric measurements were conducted within 2 h after filtration. Standards and filtrates were acidified to pH 1.5–1.7 by addition of 8 μl of 67% perchloric acid. Then 0.1 ml of 9.4 mM Fe(ClO$_4$)$_3$ solution was added to one aliquot of a split filtrate sample to achieve an Fe concentration of 302 μM. According to speciation calculations performed with MINEQL+ (Schecher and McAvoy, 1998), this Fe concentration is in excess of that required to complex all DFO-B in any filtrate analyzed. Corresponding ligand-free blank solutions, containing the background electrolyte solution, MOPS buffer, and 302 μM Fe, also were acidified to pH 1.5–1.7. Therefore, subtraction of the absorbance of a blank solution from that of a sample aliquot with Fe added yields the absorbance of the total siderophore in the sample (i.e., free siderophore ligands plus siderophore complexed with any Fe released). The net absorbance of the blank-corrected sample to which Fe was not added was attributed to Fe released by goethite dissolution during the adsorption experiments.

Samples containing both oxalic acid and DFO-B exhibited an additional absorbance peak at 288 nm. Deconvolution of the peaks at 288 and 439 nm was

necessary to determine the concentration of DFO-B accurately. This was accomplished using measurements of the molar absorptivity of oxalate and DFO-B at both wavelengths, obtained for a series of standards of each ligand in solution at pH 1.5–1.7 with the background electrolyte, MOPS buffer, and 302 μM Fe. Coupled linear equations relating the observed absorbance for an oxalate–DFO-B solution to the four molar absorptivities and the concentration of each ligand were then solved to calculate the DFO-B concentration in a sample.

Quantitation of ^{14}C-labeled oxalic acid was used to determine the concentration of oxalic acid both before the addition of solid and after filtration in the adsorption experiments. Standards containing 0.1, 0.01, 0.001, 0.0001, and 0 μCi were prepared. One milliliter of filtrate or standard solution was mixed with 14 ml of scintillation cocktail (Scintiverse, Fisher) and counted on a Beckman LS9000 Scintillation counter. For each adsorption sample, 0.1 μCi of ^{14}C-labeled oxalic acid was added. If there is no preferential adsorption of radiolabeled vs. nonlabeled oxalic acid, the ratio of residue radioactivity in the filtrate to the total radioactivity added initially represents the fraction of oxalic acid not adsorbed. Iron concentrations were determined by ICP-AES (Thermo Jarrel-Ash) using the emission line at 238.2 nm. Proton activity was measured with a Ross combination electrode calibrated with buffers at pH 4.0, 7.0, and 10.0.

## 3. Results and discussion

### 3.1. Oxalate and DFO-B adsorption

Fig. 1 shows adsorption isotherms at pH 5 for oxalate and for DFO-B on goethite in 10 mM $NaClO_4$ background electrolyte solution. Oxalate (Fig. 1a) exhibited an L-type isotherm (Sposito, 1989) that was quantified by regression analysis using a linear form of the Langmuir equation:

$$n = n_{max} - K_{ads} \frac{n}{[\ ]} \qquad (3)$$

where $n$ is surface excess, [ ] is adsorptive concentration, $n_{max}$ is an adjustable "capacity" parameter, and $K_{ads}$ is an adjustable "affinity" parameter (Fig. 1b). The maximum surface excess ($n_{max}$) was equal to
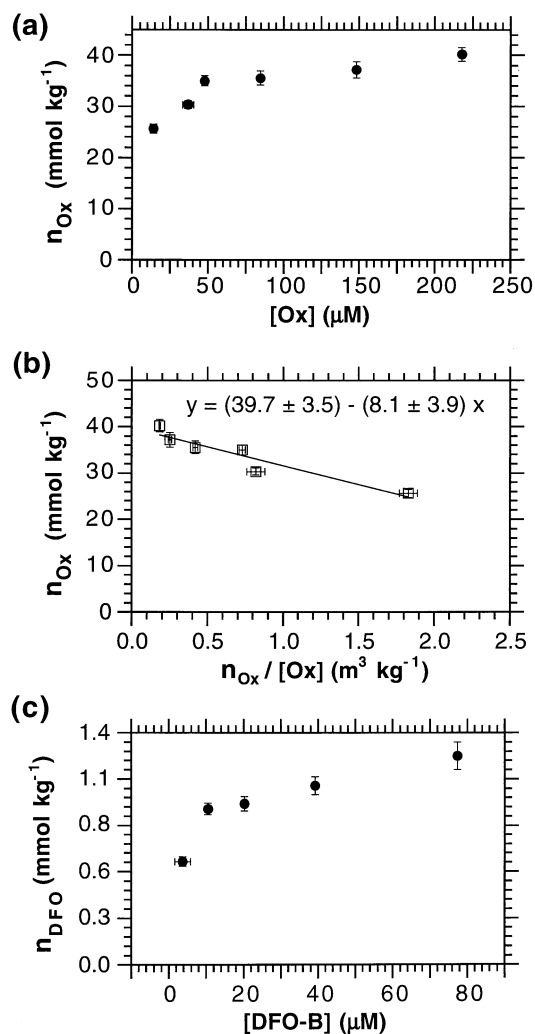


Fig. 1. (a) Adsorption isotherm for oxalate on goethite. (b) Linearized Langmuir equation fit of the oxalate adsorption data in (a) using Eq. (3). The line through the data is a least-squares adjustment [$y \equiv n$ (mmol kg$^{-1}$), $x \equiv n/[\ ]$ (m$^3$ kg$^{-1}$)]. (c) Adsorption isotherm for DFO-B on goethite ($n_{max} = 1.23 \pm 0.18$ mmol kg$^{-1}$, $K_{ads} = 3.7 \pm 2.1$ μM). Solution concentrations are those measured after 100 min in a suspension containing 10 mM $NaClO_4$, 10 g l$^{-1}$ goethite, and 5 mM MOPS buffer at pH 5. Error bars for the surface excess were calculated as described in Section 2.3, whereas those for the solution concentration reflect the range of values measured in duplicate experiments.

$40 \pm 4$ mmol kg$^{-1}$ ($1.1 \pm 0.1$ μmol m$^{-2}$), which is in agreement with previous measurements of oxalate adsorption by goethite at pH 5 reported by Zinder et al. (1986), Djafer et al. (1991), Mesuere and Fish

**(a)**



**(b)**
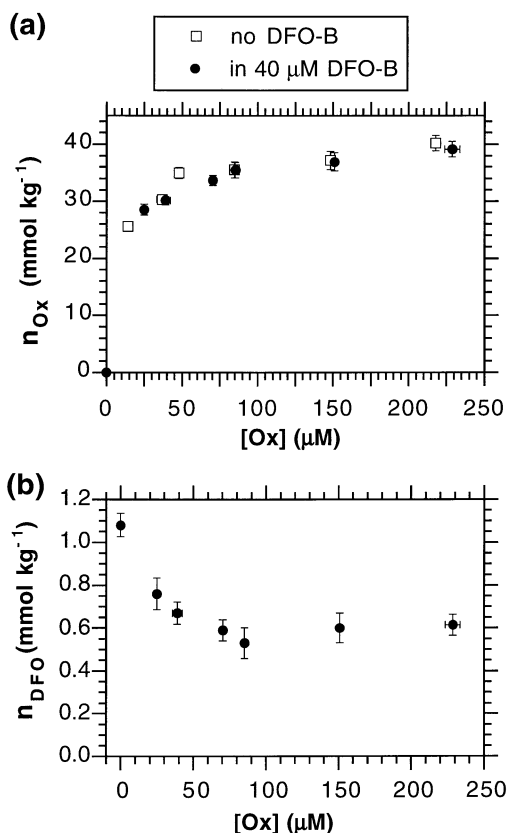
Fig. 2. Adsorption isotherms for (a) oxalate and (b) DFO-B in the presence of varying oxalate concentration and 40 µM DFO-B. Solution conditions and error estimates are the same as for Fig. 1.

(1992), and Eick et al. (1999). Adsorption of DFO-B also followed an L-type isotherm (Fig. 1c), with a Langmuir equation fit indicating a maximum surface excess ($n_{max}$) of $1.2 \pm 0.2$ mmol kg$^{-1}$ ($34 \pm 6$ nmol m$^{-2}$), in agreement with the results of Kraemer et al. (1999). They attributed this rather low $n_{max}$ value both to repulsion of the cationic DFO-B (p$K_a = 8.5$) by the positively charged goethite surface [i.e.p. ≈ 8.4 (Djafer et al., 1991); i.e.p. is the pH value at which a particle exhibits zero electrokinetic mobility (Sposito, 1998)], and to steric hindrance encountered by the siderophore while attempting to complex an Fe(III) center in the mineral. Cocozza et al. (2001) have hypothesized that both hydrophobic and stereochemical effects limit the siderophore to using just one of its three hydroxamate groups for complexing these Fe(III) centers.

Figs. 2 and 3 show adsorption isotherms at pH 5 for oxalate in the presence of 40 µM DFO-B and for DFO-B in the presence of 36 µM oxalate. As would be expected from the 30-fold disparity in surface excess (Fig. 1), oxalate adsorption was not affected by the presence of DFO-B (Fig. 2a), whereas the surface excess of DFO-B was reduced significantly as the concentration of oxalate was increased (Fig. 2b). Similarly, DFO-B adsorption was strongly affected by the presence of 36 µM oxalate (Fig. 3a), whereas the surface excess of oxalate was essentially unaffected by increasing concentrations of DFO-B, up to 80 µM (Fig. 3b). Moreover, the DFO-B adsorption isotherm in the presence of oxalate shifted from L-type to S-type (Fig. 3a), which indicates competition between oxalate and DFO-B for adsorption sites (Sposito, 1989).

Djafer et al. (1991) observed the i.e.p. of goethite to drop from 8.4 in 1 mM KNO$_3$ without oxalate to

**(a)**



**(b)**
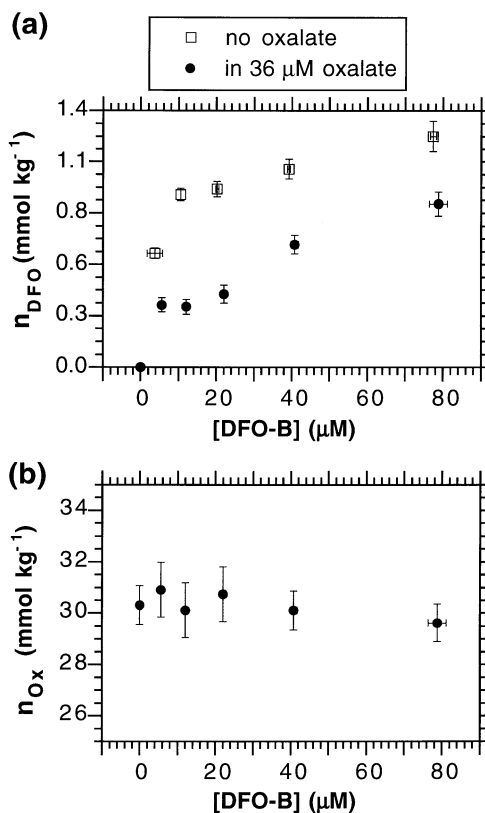
Fig. 3. Adsorption isotherms for (a) DFO-B and (b) oxalate in the presence of varying DFO-B concentration and 36 µM oxalate. Solution conditions and error estimates are the same as for Fig. 1.

7.5 or 7.0 in the presence of 10 or 100 μM oxalate, respectively. Oxalate adsorption thus lowers the surface charge on goethite, which then should facilitate adsorption of the cationic DFO-B ligand. However, the data in Figs. 2b and 3a indicate that, despite this expected enhancement, oxalate actually interfered with the adsorption of DFO-B on goethite, even when the solution concentration of DFO-B was twice that of the oxalate.

In summary, our isotherm data indicate that oxalate adsorption by goethite at pH 5 is maximal for solution concentrations above 250 μM (Fig. 1a), and is much greater than DFO-B adsorption under the same conditions. Oxalate also interferes effectively with DFO-B adsorption. These results suggest that the goethite surface sites available to DFO-B are a subset of those available to oxalate. It is possible that the much larger size of DFO-B ($M_r = 561.7$ Da) relative to oxalate ($M_r = 56$ Da) hinders DFO-B binding to the goethite surface.

## 3.2. Goethite dissolution kinetics

Fig. 4 shows graphs of the mass-normalized dissolution rate of goethite (filled circles, see also Table 1) and the surface excess of DFO-B (open triangles) both plotted against DFO-B concentration. The approximate congruence of the two graphs and the close similarity of our graph of dissolution rate vs. concentration to that reported by Liermann et al. (2000) for DFO-B-promoted hornblende dissolution lend credence to an interpretation of the data as evidence for DFO-B-promoted goethite dissolution kinetics. A pseudo first-order rate coefficient (units of $h^{-1}$) for ligand-promoted dissolution is conventionally calculated as the ratio of the mass-normalized dissolution rate to the surface excess (Zinder et al., 1986). The data in Fig. 4a at DFO-B concentrations of 20, 40, and 80 μM yield an average value of $0.015 \pm 0.003$ $h^{-1}$ for this rate coefficient, in agreement with pseudo first-order rate coefficients that can be calculated using kinetics data reported by Watteau and Berthelin (1994) and Kraemer et al. (1999) for DFO-B-promoted dissolution of goethite at circumneutral pH.

The above calculation is made under the assumption that the proton-promoted dissolution rate of goethite under our experimental conditions is negligible. This assumption can be tested statistically by
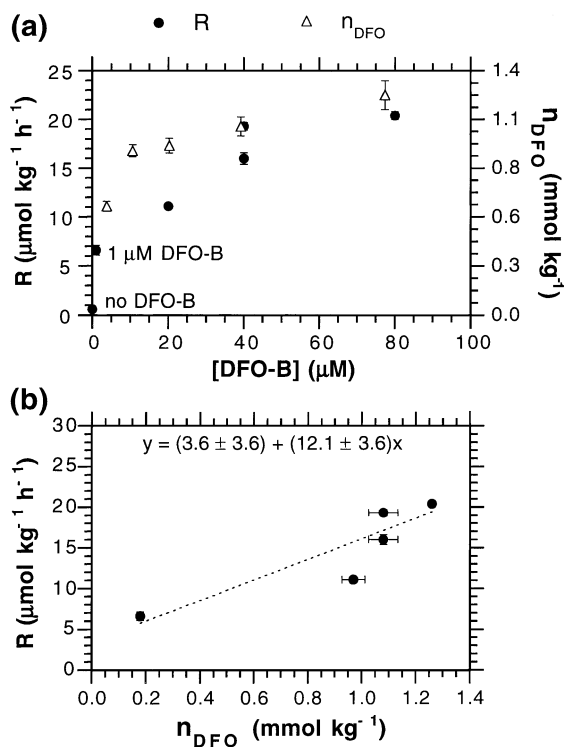


Fig. 4. (a) Mass-normalized dissolution rate of goethite and surface excess of DFO-B plotted together as a function of DFO-B solution concentration. Each dissolution rate represents a separate experiment in which steady-state Fe concentrations and reactor flow rates were averaged over several days to calculate $R$ as in Eq. (1). Error bars represent $\Delta R$ as in Eq. (2). Error bars for the surface excess were calculated as described in Fig. 1. Solution conditions: 10 mM $NaClO_4$, 10 g $l^{-1}$ goethite, 5 mM MOPS buffer, pH 5. (b) Plot of the dissolution rate in (a) vs. the surface excess of DFO-B. The line through the data is a least-squares fit [$y \equiv R$ (μmol $kg^{-1}$ $h^{-1}$), $x \equiv n$ (mmol $kg^{-1}$)] with 95% confidence limits indicated for the slope and $y$-intercept. The smallest surface excess value, 0.18 mmol $kg^{-1}$, which corresponds to 1 μM dissolved DFO-B, was calculated using the Langmuir model in Eq. (3) with the parameters, $n_{max} = 1.23$ mmol $kg^{-1}$, $K_{ads} = 3.7$ μM, found from analyzing the data in Fig. 1c.

plotting the dissolution rates in Fig. 4a against the surface excess and observing whether the $y$-intercept is zero [see e.g., the inset in Fig. 6 of Zinder et al. (1986)]. The result of this exercise (Fig. 4b) was a statistically significant linear relationship whose slope was $0.012 \pm 0.004$ $h^{-1}$, in agreement with the pseudo first-order rate coefficient calculated above. The $y$-intercept was $3.6 \pm 3.6$ μmol $kg^{-1}$ $h^{-1}$, which does not differ statistically from the value 0.

Table 1
Calculation of $\Delta_r G$ [Eq. (5)] for goethite dissolution at pH 5 in the presence of DFO-B and oxalate (solution conditions: 10 g $l^{-1}$ goethite, 10 mM NaClO$_4$, 5 mM buffer)

| [DFO-B] ($\mu$M) | [Ox] ($\mu$M) | pH | Flow rate (ml h$^{-1}$) | [Fe]$_{eff}$ ($\mu$M) | R ($\mu$mol kg$^{-1}$ h$^{-1}$) | $\Delta_r G$ (kJ mol$^{-1}$) |
|---|---|---|---|---|---|---|
| 0 | 70 | 4.90 | 2.30 | 0.18 | 0.7 | 2.3[a] |
| 0 | 100 | 5.15 | 10.68 | 0.35 | 5.3 | 5.4 |
| 0 | 200 | 4.98 | 10.40 | 1.19 | 17.9 | 1.1 |
| 0 | 200 | 5.00 | 5.25 | 1.90 | 14.3 | 2.3 |
| 0 | 200 | 5.00 | 1.02 | 2.21 | 3.3 | 2.6 |
| 0 | 750 | 5.00 | 8.25 | 4.10 | 48.7 | − 5.0 |
| 0 | 750 | 5.00 | 9.36 | 4.46 | 60.1 | − 4.8 |
| 0 | 1250 | 5.00 | 9.37 | 5.71 | 77.2 | − 7.9 |
| 0 | 2000 | 5.00 | 8.46 | 10.35 | 126.2 | − 9.9 |
| 0 | 3000 | 5.00 | 9.42 | 9.09 | 123.5 | − 13.2 |
| 0 | 3000 | 5.00 | 8.89 | 9.50 | 121.8 | − 13.1 |
| 0 | 5000 | 5.00 | 8.52 | 14.08 | 172.9 | − 15.9 |
| 0 | 8000 | 5.00 | 8.97 | 12.63 | 163.3 | − 19.6 |
| 0 | 8000 | 5.00 | 8.85 | 12.90 | 164.6 | − 19.5 |
| 1 | 0 | 5.01 | 9.16 | 0.50 | 6.6 | − 15.1 |
| 20 | 0 | 5.11 | 10.11 | 0.80 | 11.6 | − 23.0 |
| 40 | 0 | 4.73 | 7.75 | 1.40 | 16.0 | − 23.4 |
| 40 | 0 | 5.11 | 9.70 | 1.33 | 19.3 | − 23.5 |
| 40 | 0 | 5.11 | 5.82 | 2.43 | 19.3 | − 21.9 |
| 80 | 0 | 4.96 | 2.87 | 4.93 | 20.4 | − 21.9 |
| 10 | 40 | 4.96 | 2.90 | 8.83 | 36.7 | − 10.1 |
| 20 | 40 | 5.11 | 12.47 | 2.05 | 37.0 | − 20.5 |
| 40 | 40 | 5.13 | 11.63 | 2.50 | 42.0 | − 21.8 |
| 40 | 40 | 5.24 | 9.04 | 2.96 | 38.9 | − 21.4 |
| 1 | 28.6 | 5.02 | 9.65 | 0.91 | 12.7 | − 9.3 |
| 5 | 28.6 | 5.08 | 11.97 | 2.57 | 44.3 | − 15.0 |
| 80 | 28.6 | 5.27 | 10.16 | 2.08 | 30.5 | − 24.1 |
| 40 | 10 | 5.25 | 6.35 | 2.02 | 18.4 | − 22.4 |
| 40 | 10 | 5.25 | 10.40 | 1.71 | 25.6 | − 22.8 |
| 40 | 14.3 | 5.17 | 10.55 | 1.76 | 26.8 | − 22.8 |
| 40 | 20 | 5.05 | 11.87 | 1.93 | 33.1 | − 22.5 |
| 40 | 50 | 5.09 | 2.02 | 12.11 | 35.4 | − 17.2 |
| 40 | 100 | 4.89 | 6.74 | 4.56 | 44.4 | − 20.2 |
| 40 | 142.8 | 5.22 | 9.28 | 4.22 | 56.4 | − 20.4 |

[a] First five values listed do not differ statistically from the value 0.

Fig. 5 shows the mass-normalized dissolution rate of goethite at pH 5 plotted against oxalate concentration. The overall shape of the graph is sigmoid (Fig. 5a), ultimately becoming convex at very high oxalate concentrations above 1 mM (Fig. 5b). At oxalate concentrations below 200 $\mu$M, the dissolution rate is much smaller than that measured in the presence of DFO-B (Fig. 4a) at the same pH and ligand concentration. Moreover, the dissolution data in Fig. 5a are not congruent with the oxalate adsorption isotherm in Fig. 1a. Therefore, the dissolution rate–concentration relationship for oxalate in Fig. 5a cannot be interpreted in terms of the surface excess of oxalate, which in any case should be essentially constant over the oxalate concentration range of 100 $\mu$M to 8 mM.

Instead, it is likely that the steady-state dissolution rates plotted in Fig. 5 mainly reflect the physical removal of Fe from the reactor because of rapid equilibration of the solid phase with the oxalate solutions. In separate experiments at a fixed oxalate concentration of 200 $\mu$M, we observed a proportional increase of the dissolution rate with increasing flow rate in the reactor (Fig. 6a), and the values of [Fe]$_{eff}$ we measured, within their precision and that of the thermodynamic data, were not significantly different from total soluble Fe calculated using MINEQL+
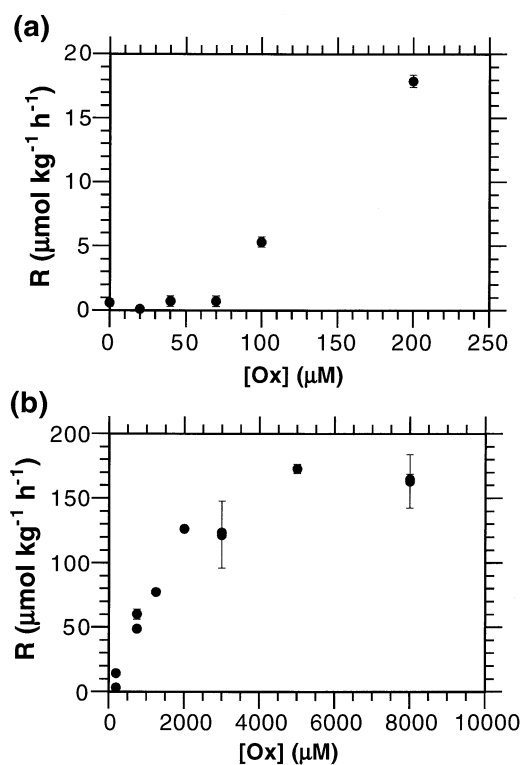


Fig. 5. Mass-normalized dissolution rate of goethite as a function of oxalate solution concentration: (a) 0–250 $\mu$M range, (b) 0–8 mM range. Solution conditions and error estimates are the same as in Fig. 4.
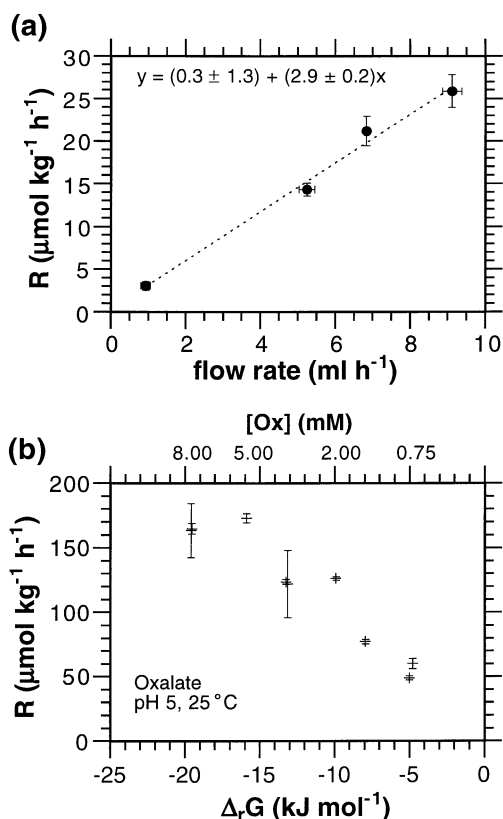
Fig. 6. (a) Mass-normalized dissolution rate of goethite as a function of the flow rate in the stirred tank reactor. The line through the data is a least-squares fit [$y \equiv R$ (µmol kg$^{-1}$ h$^{-1}$), $x \equiv$ flow rate (ml h$^{-1}$)]. Solution conditions and error estimates are as in Fig. 4. (b) Values of $\Delta_r G$ [Eq. (5)] for goethite dissolution at pH 5 with oxalate concentrations in the range 0.75–8.00 mM. Corresponding values of the oxalate concentration are labeled approximately on the graph.

using the standard equation (Lasaga, 1998):

$$\Delta_r G = \mathbf{R}T\ln\frac{Q}{K_{eq}} \qquad (5)$$

where $\mathbf{R}$ is the molar gas constant, $T$ is absolute temperature, $Q = (Fe^{3+})/(H^+)^3$, and $K_{eq} = 10^{0.36}$ is the equilibrium constant for the dissolution reaction, respectively. The activity quotient $Q$ was calculated with measured pH values and total dissolved iron concentrations ([Fe]$_{eff}$) as input to MINEQL + (Schecher and McAvoy, 1998) using the equilibrium constants in Table 2. Uncertainty in the estimates of $\Delta_r G$ was calculated based on the imprecision in log $K_{eq}$ and those in the laboratory measurements of [Fe]$_{eff}$ and pH. This calculation was similar to that of the uncertainty in dissolution rates depicted in Eq. (2). Within the estimated uncertainty of $\Delta_r G$ (2−5 kJ mol$^{-1}$), saturation conditions existed for oxalate concentrations at or below 200 µM (Table 1, top five rows). Undersaturation ($\Delta_r G < 0$) occurred when the oxalate con-

Table 2

Thermodynamic formation constants for DFO-B, oxalate, and Fe(III) species at 298.15 K (infinite dilution reference state)

| Reaction | log $K_{298}$ |
|---|---|
| $DFOB^{3-} + H^+ = HDFOB^{2-}$ | 10.01[a] |
| $DFOB^{3-} + 2H^+ = H(HDFOB)^-$ | 19.00[a] |
| $DFOB^{3-} + 3H^+ = H_2(HDFOB)^0$ | 27.73[a] |
| $DFOB^{3-} + 4H^+ = H_3(HDFOB)^+$ | 36.24[a] |
| $FeDFOB^0 + H^+ = Fe(HDFOB)^+$ | 10.40[a] |
| $DFOB^{3-} + H^+ + Fe^{3+} = Fe(HDFOB)^+$ | 38.55[b] |
| $DFOB^{3-} + 2H^+ + Fe^{3+} = FeH(HDFOB)^{2+}$ | 39.12[b] |
| $DFOB^{3-} + 3H^+ + Fe^{3+} = FeH_2(HDFOB)^{3+}$ | 39.83[b] |
| $C_2O_4^{2-} + H^+ = HC_2O_4^-$ | 4.266[a] |
| $C_2O_4^{2-} + 2H^+ = H_2C_2O_4^0$ | 1.252[a] |
| $C_2O_4^{2-} + Fe^{3+} = FeC_2O_4^+$ | 8.80[a] |
| $2C_2O_4^{2-} + Fe^{3+} = Fe(C_2O_4)_2^-$ | 15.44[a] |
| $3C_2O_4^{2-} + Fe^{3+} = Fe(C_2O_4)_3^{3-}$ | 19.83[a] |
| $H_2O + Fe^{3+} = FeOH^{2+} + H^+$ | − 2.19[a] |
| $2H_2O + Fe^{3+} = Fe(OH)_2^+ + 2H^+$ | − 4.69[a] |
| $2H_2O + Fe^{3+} = FeOOH(s) + 3H^+$ | − 0.36[c] |

[a] Conditional formation constant from Martell et al. (1998), corrected to zero ionic strength with the Davies equation (Sposito, 1989).
[b] Conditional formation constant from Biruš et al. (1987), corrected to zero ionic strength with the Davies equation.
[c] Thermodynamic formation constant for goethite from Parker and Khodakovskii (1995); log $K_{eq}$ uncertainty $\approx \pm 0.35$. Robie and Hemingway (1995) provide independent thermodynamic data yielding log $K_{eq} = - 0.16 \pm 0.49$, which does not differ statistically from the value listed here.

(Schecher and McAvoy, 1998) based on oxalate protonation and Fe(III) complexation reactions, Fe(III) hydrolysis reactions, and the goethite formation reaction listed in Table 2 (bottom eight reactions). The speciation results also showed all of the dissolved Fe(III) in equilibrium with goethite to be complexed with oxalate, mostly (86%) as the species $Fe(C_2O_4)_3^{3-}$.

Speciation calculations also were used to examine the extent of equilibration of the reaction:

$$\alpha - FeOOH(s) + 3H^+ = Fe^{3+} + 2H_2O(\ell)$$
$$\log K_{eq} = 0.36 \pm 0.35 \qquad (4)$$

centration exceeded 750 μM (Fig. 6b and Table 1). At oxalate concentrations above 5 mM, the dissolution rate appeared to be reaching a plateau suggesting far-from-equilibrium conditions, as found previously for goethite dissolution (Kraemer and Hering, 1997).

Fig. 7 shows the mass-normalized dissolution rate of goethite at pH 5 in the presence of varying concentrations of DFO-B at three fixed concentrations of oxalate (Fig. 7a), and in the presence of varying concentrations of oxalate at two fixed concentrations of DFO-B (Fig. 7b). The dissolution rate promoted by DFO-B (Fig. 7a) is approximately doubled when oxalate is present at equimolar concentrations (29 and 40 μM DFO-B), whereas that in the presence of

oxalate (Fig. 7b) is increased by more than an order of magnitude when DFO-B is present at an equimolar concentration (40 μM oxalate). At oxalate concentrations above 80 μM, the dissolution rate in the presence of 40 μM DFO-B parallels that in the absence of DFO-B (Fig. 7b).

### 3.3. Dissolution mechanisms

The kinetics and adsorption data in Fig. 4 are consistent with a conventional model rate law for ligand-promoted dissolution (Stumm et al., 1983):

$$R_{DFO} = k_{DFO}n_{DFO} \qquad (6)$$

where $R_{DFO}$ is the mass-normalized rate of steady-state dissolution [Eq. (1)], $k_{DFO} = 0.015$ h$^{-1}$ is a pseudo first-order rate coefficient, and $n_{DFO}$ is the surface excess of DFO-B (Fig. 1c). The rate coefficient in Eq. (6) is, in principle, an implicit function of all variables, other than $n_{DFO}$, which affect $R_{DFO}$ (e.g., pH, temperature, composition). When oxalate is present, as the kinetics data in Fig. 7a show, $R_{DFO}$ increases by a factor of two or more. Associated with this increase is the adsorption of oxalate and a substantial desorption of DFO-B (Fig. 3). These facts suggest that, in the mixed-ligand system, the rate law in Eq. (6) becomes:

$$R = k_{DFO}^{Ox}n_{DFO}^{Ox} + k_{Ox}^{DFO}n_{Ox}^{DFO} \qquad (7)$$

In order to reflect the possible influence of one ligand on the other, the two pseudo first-order rate coefficients in Eq. (7) are labeled with a subscript denoting a dissolution-promoting ligand and a superscript denoting its competitor. These rate coefficients should not be affected by ligand competition for adsorption sites because this is already taken into account in the surface excess quantities, ($n_{DFO}^{Ox}$ and $n_{Ox}^{DFO}$), which are measured in the two-ligand system.

The rate law in Eq. (7) applies to parallel reactions far from equilibrium. The data in Figs. 3 and 7a can be used to deduce a value for the pseudo first-order rate coefficient $k_{Ox}^{DFO}$ under the assumption that $k_{DFO}^{Ox} = k_{DFO}$. This assumption implies that the sole effect of oxalate on the interaction between DFO-B and goethite is to reduce the surface excess of DFO-B, without altering the basic mechanism of DFO-B-promoted dissolution. On subtracting the
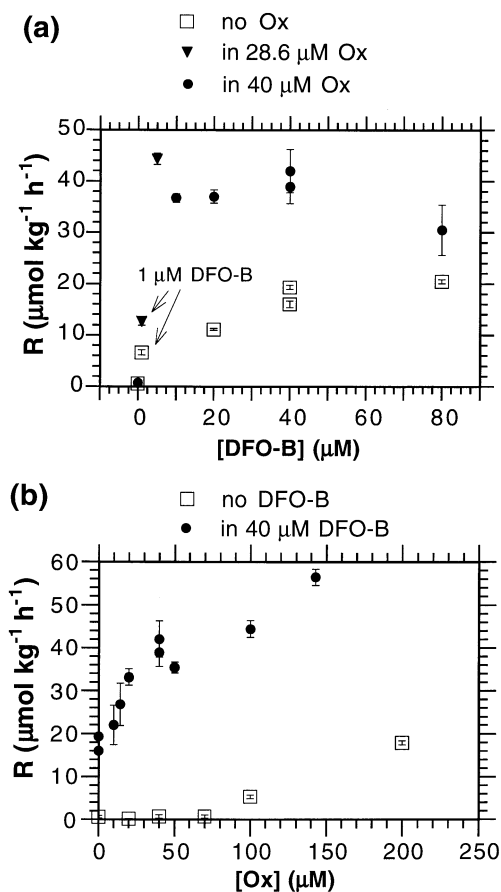


Fig. 7. Mass-normalized dissolution rate of goethite as a function of: (a) DFO-B solution concentration at three oxalate concentrations, (b) oxalate concentration at two DFO-B concentrations. Solution conditions as in Fig. 4.
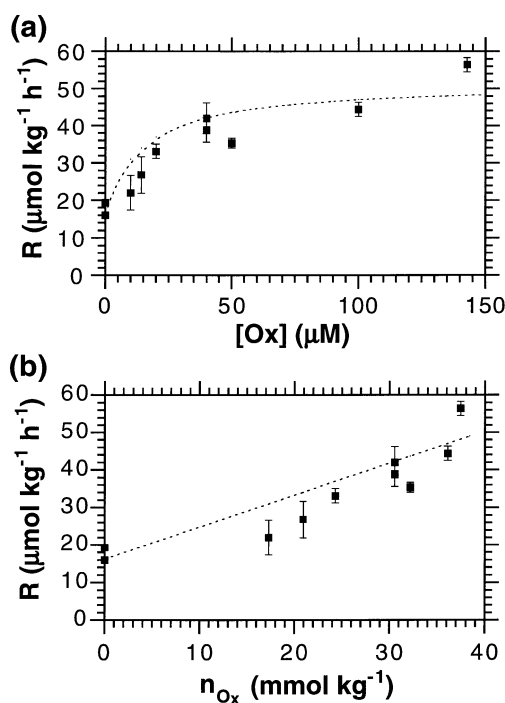
Fig. 8. Comparison between experimental (■) and calculated (dotted) mass-normalized dissolution rates of goethite in the presence of 40 μM DFO-B and varying solution concentrations of oxalate: (a) rate of dissolution vs. oxalate solution concentration, (b) rate of dissolution vs. surface excess of oxalate. The calculated rates are based on Eq. (7) with $k_{DFO}^{Ox} = 0.015$ h$^{-1}$ and $k_{Ox}^{DFO} = 0.001$ h$^{-1}$ (no adjustable parameters).

first term on the right side of Eq. (7) [calculated with observed values of $n_{DFO}^{Ox}$ (Fig. 3a)] from the observed dissolution rate, then dividing the result by the measured values of $n_{OX}^{DFO}$ in Fig. 3b, one finds $k_{Ox}^{DFO} \approx 0.001$ h$^{-1}$ with a coefficient of variation of about 20%.

A test of the rate law in Eq. (7) [with $k_{DFO}^{Ox} = 0.015$ h$^{-1}$ and $k_{Ox}^{DFO} = 0.001$ h$^{-1}$] using the adsorption data in Fig. 2 (variable oxalate concentration, 40 μM DFO-B) appears plotted in two ways in Fig. 8. The dissolution rates are those measured in the presence of variable oxalate concentrations at 40 μM DFO-B (Fig. 7b). It is apparent that Eq. (7) provides a reasonable quantitative description of the dissolution kinetics in a system with variable oxalate concentration and a fixed DFO-B concentration, after calibration in a system with variable DFO-B concentration and a fixed oxalate concentration.

A question may be raised as to why a far-from-equilibrium rate law [Eq. (7)] is applicable to mixed oxalate–DFO-B systems, and to a single-ligand system containing DFO-B alone [Eq. (6)], but not to a single-ligand system containing oxalate alone. For this latter system, far-from-equilibrium conditions do not obtain until the oxalate concentration exceeds 5 mM (Fig. 6b). Insight once again can be obtained by doing a chemical affinity ($\Delta_r G$) calculation based on the experimental conditions for the systems containing DFO-B. As shown in Table 1, even at the lowest DFO-B concentration used in our experiments (1 μM), $\Delta_r G < -9$ kJ mol$^{-1}$, indicating undersaturation conditions. Moreover, there is no apparent dependence of the dissolution rates on $\Delta_r G$, confirming that all of the systems in which DFO-B was present were indeed at far-from-equilibrium conditions, irrespective of whether oxalate was present.

The applicability of a far-from-equilibrium rate law [Eq. (7)] to the mixed oxalate–DFO-B system now can be elucidated further by a speciation calculation for a mixed oxalate–DFO-B solution containing dissolved Fe(III) at pH 5. Table 3 presents the results of such a calculation, based on the first 15 reactions listed in Table 2, for a solution containing 1 μM dissolved Fe(III), 40 μM oxalate, and 40 μM DFO-B at pH 5 and 10 mM ionic strength. It is evident that all of the dissolved Fe(III) is in the soluble complex Fe(HDFOB)$^+$. This same result was found after reducing the DFO-B concentration to 1 μM while maintaining those of Fe(III) and oxalate at their previous values (data not shown). Therefore, so long as the concentration of DFO-B is large enough to capture all the dissolved Fe(III) released by goethite

Table 3
Principal speciation in an aqueous solution comprising 1 μM Fe(III), 40 μM DFO-B, and 40 μM oxalate at pH 5 and 10 mM ionic strength, as calculated by MINEQL+ (Schecher and McAvoy, 1998)[a]

| Species | Concentration (μM) | Species | Concentration (μM) |
|---|---|---|---|
| H$_3$(HDFOB)$^+$ | 39.0 | C$_2$O$_4^{2-}$ | 35.2 |
| Fe(HDFOB)$^+$ | 1.0 | HC$_2$O$_4^-$ | 4.8 |

[a] Based on the thermodynamic data in Table 1. In the case of 1 μM DFO-B total concentration, the concentration of H$_3$(HDFOB)$^+$ drops to 4.6 nM while all other species concentrations remain the same.

dissolution, this ligand will wrest Fe(III) from any Fe−oxalate complexes that may have formed, leaving an uncomplexed oxalate ligand available to react with again the goethite surface. From the perspective of the oxalate ligand, therefore, the system is indeed far from equilibrium.

The implications of Eqs. (6) and (7) for the microbial acquisition of Fe from goethite are most interesting. It has long been known that DFO-B, by virtue of its large affinity for Fe, can affect the amount of bioavailable Fe [see e.g., Neilands, 1974]. Eqs. (6) and (7) illustrate two mechanisms through which this affinity can affect Fe release kinetics. Eq. (6) shows that DFO-B alone can modestly increase the rate of goethite dissolution in the absence of other ligands (ligand-promoted dissolution). However, in reality, for soils and other biologically active environments, a variety of organic ligands is always present, with oxalate being the most common (Gadd, 2000). The relevance of Eq. (7) for the microbial acquisition of Fe then becomes apparent. For example, the data in Figs. 5b and 7a indicate that comparable rates of goethite dissolution are to be expected in the presence of either 500 μM oxalate or just 40 μM oxalate combined with only 10 μM DFO-B, despite the fact that negligible dissolution occurs in the presence of 40 μM oxalate alone, and rather little in the presence of 10 μM DFO-B alone. Oxalate adsorption onto goethite at 40 μM concentration is at about 70% of its maximal value (Fig. 1a), thereby providing a rich potential source of soluble Fe if the driving force for continual Fe−oxalate detachment from the goethite surface could somehow be increased. Adding a small concentration of predatory DFO-B ligands, which have little propensity to be lost from solution by adsorption (Fig. 1c), can serve this purpose by depleting the aqueous solution phase of Fe−oxalate complexes, thus increasing the thermodynamic pressure for Fe−oxalate desorption. The remarkable advantage that accrues to the microbial producer of the siderophore also can be inferred from Fig. 7a, which implies that DFO-B concentrations well in excess of 100 μM would be required in order to achieve the same dissolution rate as is observed in the presence of only 10 μM DFO-B, and with just enough oxalate present to adsorb abundantly while serving as prey for the siderophore.

## References

Albrecht-Gary, A.-M., Crumbliss, A.L., 1998. Coordination chemistry of siderophores: thermodynamics and kinetics of iron chelation and release. In: Sigel, A., Sigel, H. (Eds.), Iron Transport and Storage in Microorganisms, Plants, and Animals. Marcel Dekker, New York, pp. 239–327.

Biruš, M., Bradić, Z., Krznarić, G., Kujundžic, N., Pribanić, M., Wilkins, P.C., Wilkins, R.G., 1987. Kinetics of stepwise hydrolysis of ferrioxamine B and of formation of diferrioxamine B in acid perchlorate solution. Inorg. Chem. 26, 1000–1005.

Cocozza, C., Tsao, C.C.G., Cheah, S.-F., Kraemer, S.M., Raymond, K.N., Miano, T.M., Sposito, G., 2001. Temperature dependence of goethite dissolution promoted by trihydroxamate siderophores. Geochim. Cosmochim. Acta 66, 431–438.

Cornell, R.M., Schwertmann, U., 1996. The Iron Oxides. VCH Publishers, Weinheim.

Crumbliss, A.L., 1991. Aqueous solution equilibrium and kinetic studies of iron siderophore and model siderophore complexes. In: Winkelmann, G. (Ed.), Handbook of Microbial Iron Chelates. CRC Press, Boca Ratón, FL, pp. 177–232.

Djafer, M., Khandal, R.K., Terce, M., 1991. Interactions between different anions and the goethite surface as seen by different methods. Colloids Surf. 54, 209–218.

Eick, M.J., Peak, J.D., Brady, W.D., 1999. The effect of oxyanions on the oxalate-promoted dissolution of goethite. Soil Sci. Soc. Am. J. 63, 1133–1141.

Gadd, G.M., 2000. Heterotrophic solubilization of metal-bearing minerals by fungi. In: Cotter-Howells, J.D., Campbell, L.S., Valsami-Jones, E., Batchelder, M. (Eds.), Environmental Mineralogy. The Mineralogical Society, London, pp. 57–75.

Holmén, B.A., Casey, W.H., 1996, 1998. Hydroxamate ligands, surface chemistry, and the mechanism of ligand-promoted dissolution of goethite [α-FeOOH(s)]. Geochim. Cosmochim. Acta 60, 4403–4415; 62, 726.

Kalinowski, B.E., Liermann, L.J., Givens, S., Brantley, S.L., 2000. Rates of bacteria-promoted solubilization of Fe from minerals: a review of problems and approaches. Chem. Geol. 169, 357–370.

Kraemer, S.M., Hering, J.G., 1997. Influence of solution saturation state on the kinetics of ligand-controlled dissolution of oxide phases. Geochim. Cosmochim. Acta 61, 2855–2866.

Kraemer, S.M., Cheah, S.-F., Zapf, R., Xu, J., Raymond, K.N., Sposito, G., 1999. Effect of hydroxamate siderophores on Pb(II) adsorption and Fe release by goethite. Geochim. Cosmochim. Acta 63, 3003–3008.

Lasaga, A.C., 1998. Kinetic Theory in the Earth Sciences. Princeton Univ. Press, Princeton, NJ.

Liermann, L.J., Kalinowski, B.E., Brantley, S.L., Ferry, J.G., 2000. Role of bacterial siderophores in dissolution of hornblende. Geochim. Cosmochim. Acta 64, 587–602.

Martell, A.E., Smith, R.M., Motekaitis, R.J., 1998. Critically Selected Stability Constants of Metal Complexes Database. NIST, Gaithersburg, MD.

Mesuere, K., Fish, W., 1992. Chromate and oxalate adsorption on goethite: 1. Calibration of surface complexation models. Environ. Sci. Technol. 26, 2357–2364.

Nagy, K.L., Blum, A.E., Lasaga, A.C., 1991. Dissolution and precipitation kinetics of kaolinite at 80 °C and pH 3: the dependence on solution saturation state. Am. J. Sci. 291, 649–686.

Neilands, J.B., 1974. Iron and its role in microbial physiology. In: Neilands, J.B. (Ed.), Microbial Iron Metabolism. Academic Press, New York, pp. 3–34.

Parker, V.B., Khodakovskii, I.L., 1995. Thermodynamic properties of the aqueous ions (2+ and 3+) of iron and the key compounds of iron. J. Phys. Chem. Ref. Data 24, 1699–1745.

Robie, R.A., Hemingway, B.S., 1995. Thermodynamic Properties of Minerals and Related Substances at 298.15 K and 1 Bar ($10^5$ Pascals) Pressure and Higher Temperatures. U.S. Geol. Surv. Bull. 2131. U.S. Government Printing Office, Washington, DC.

Schecher, W.D., McAvoy, D.C., 1998. MINEQL+, A Chemical Equilibrium Modeling System. Environmental Research Software, Hallowell, ME.

Schwertmann, U., Cornell, R.M., 1991. Iron Oxides in the Laboratory. VCH Publishers, Weinheim.

Soares, H.M.V.M., Conde, P.C.F.L., Almeida, A.A.N., Vasconcelos, M.T.S.D., 1999. Evaluation of *n*-substituted aminosulfonic acid buffer with a morpholino ring for cadmium and lead speciation studies by electroanalytical techniques. Anal. Chim. Acta 394, 325–335.

Solinas, V., 1994. Cation effects on the adsorption of desferrioxamine B (DFOB) by humic acid. In: Senesi, N., Miano, T.M. (Eds.), Humic Substances in the Global Environment and Implications on Human Health. Elsevier, Amsterdam, pp. 1183–1188.

Sposito, G., 1989. The Chemistry of Soils. Oxford Univ. Press, New York.

Sposito, G., 1998. On points of zero charge. Environ. Sci. Technol. 32, 2815–2819.

Stumm, W., Furrer, G., Kunz, B., 1983. The role of surface coordination in precipitation and dissolution of mineral phases. Croat. Chem. Acta 56, 593–611.

Watteau, F., Berthelin, J., 1994. Microbial dissolution of iron and aluminum from soil minerals: efficiency and specificity of hydroxamate siderophores compared to aliphatic acids. Eur. J. Soil Biol. 30, 1–9.

Yu, Q., Kandegedara, A., Xu, Y., Rorabacher, D.B., 1997. Avoiding interferences from Good's buffers: a contiguous series of noncomplexing tertiary amine buffers covering the entire range of pH 3–11. Anal. Biochem. 253, 50–56.

Zinder, B., Furrer, G., Stumm, W., 1986. The coordination chemistry of weathering: II. Dissolution of Fe(III) oxides. Geochim. Cosmochim. Acta 50, 1861–1869.